Mixing and Energetics of the Oceanic Thermohaline Circulation*

RUI XIN HUANG

Department of Physical Oceanography, Woods Hole Oceanographic Institution, Woods Hole, Massachusetts

(Manuscript received 23 July 1997, in final form 20 May 1998)

ABSTRACT

Using an idealized tube model and scaling analysis, the physics supporting the oceanic thermohaline circulation is examined. Thermal circulation in the tube model can be classified into two categories. When the cooling source is at a level higher than that of the heating source, the thermal circulation is friction-controlled; thus, mixing is not important in determining the circulation rate. When the cooling source is at a level lower than that of the heating source, the circulation is mixing controlled; thus, weak (strong) mixing will lead to weak (strong) thermal circulation.

Within realistic parameter regimes the thermohaline circulation requires external sources of mechanical energy to support mixing in order to maintain the basic stratification. Thus, the oceanic circulation is only a heat conveyor belt, not a heat engine. Simple scaling shows that the meridional mass and heat fluxes are linearly proportional to the energy supplied to mixing.

The rate of tidal dissipation in the open oceans (excluding the shallow marginal seas) is about 0.9–1.3 ($\times 10^{12}$ W); the rate of potential energy generated by geothermal heating is estimated to be 0.5×10^{12} W. Accordingly, the global-mean rate of mixing inferred from oceanic climatological data is about 0.22×10^{-4} m^2 s^{-1}.

Using a primitive equation model, numerical experiments based on a fixed energy source for mixing have been carried out in order to test the scaling law. In comparison with models under fixed rate of mixing, a model under a fixed energy for mixing is less sensitive to changes in the forcing conditions due to climatic changes. Under a surface relaxation condition for temperature and standard parameters, the model is well within the region of Hopf bifurcation, so decadal variability is expected.

1. Introduction

The energetics of the oceanic circulation seems to be a very unpopular subject. One day when I met a former student of mine, he made an interesting comment: ''It is very nice that we don't have to worry about the energy equation in oceanography.'' His comment sounds quite similar to that of drivers on highways: ''Do you need anything?'' ''Not really!'' In fact, whenever we drive on highways, we need gasoline and air as the energy source to support the car engine.

The common practice in oceanic general circulation modeling is to choose a diapycnal mixing rate and let the model run; the diapycnal mixing rate remains the same all the time, even under different climatic conditions. In fact, no modelers have ever checked how much energy is required to support mixing and circulation, and, most importantly, whether this amount of energy is really available.

The oceanic thermohaline circulation is predominately forced by heating/cooling at the surface. Although freshwater flux also contributes to the thermohaline circulation, its interaction with thermal forcing is complicated, and it may enhance or reduce the circulation driven by thermal forcing alone. In simple models, both the thermal and saline forcing can be treated in terms of a combined buoyancy force. Since in most cases thermal forcing is the dominating component, traditionally the oceanic circulation has been treated as a heat engine. The physical mechanisms determining the oceanic thermal circulation have been discussed many times over the past hundred years.

Sandstrom (1916) considered the momentum balance of the steady circulation in the oceans. To overcome friction, there should be a net input of mechanical energy over each closed streamline

$$w = -\int_s v\, dp > 0, \tag{1}$$

where v and p are the specific volume and pressure, respectively, and the integration is taken along closed streamlines s. He simplified the oceanic circulation in

* Woods Hole Oceanographic Institution Contribution Number 9405.

Corresponding author address: Dr. Rui Xin Huang, Department of Physical Oceanography, Woods Hole Oceanographic Institution, Woods Hole, MA 02543.
E-mail: rhuang@whoi.edu

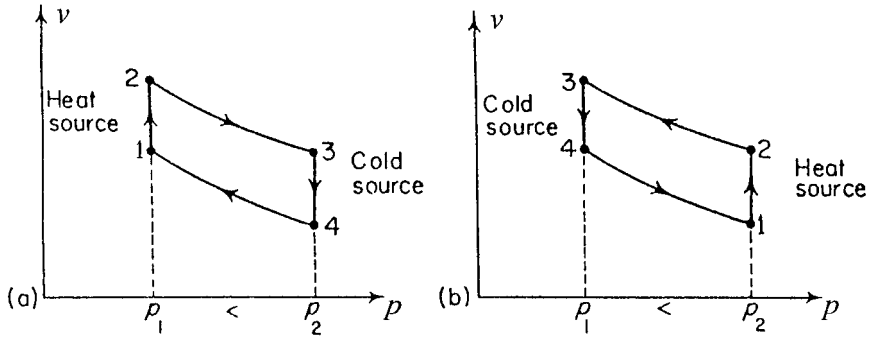

FIG. 1. An idealized Carnot cycle for the oceanic heat engine, as proposed by Sandstrom [adapted from Defant (1961)].

terms of a heat engine by assuming four idealized stages within each cycle of the oceanic heat engine: i) heating-induced expansion under a constant pressure; ii) adiabatic transition from the heating source to the cooling source; iii) cooling-induced contraction under a constant pressure; and iv) adiabatic transition from the cooling source to the heating source.

According to this idealized cycle, the net amount of work would be negative, if the system is heated under low pressure, but cooled under high pressure (Fig. 1a). Positive work is possible only for the counterclockwise cyclic process, in which heating takes place at a higher pressure and cooling takes place at a lower pressure, as shown in Fig. 1b. Thus, he came to the conclusion, here referred to as

Sandstrom's Theorem: A closed steady circulation can be maintained in the ocean only if the heating source is situated at a lower level than the cooling source.

In order to illustrate his theorem, Sandstrom carried out laboratory experiments. In the first experiment, the heating source was put at a level lower than the cooling source. Strong circulation was observed between the levels of heating and cooling. In the second experiment, the heating source was put at a level higher than the cooling source. No circulation was observed, and a stable stratification was observed between the heating and cooling levels.

Sandstrom's theorem was questioned by Jeffreys (1925), who pointed out that any horizontal density (temperature) gradient must induce a circulation. By including the diffusion terms in the density balance equation, Jeffreys concluded that a circulation should be induced even if the heating source were put at a level higher than the cooling source.

The debate over Sandstrom's theorem continues to the present time. Further reference to Sandstrom's theorem may be found in many books and review articles, for example, Hodske et al. (1957), Defant (1961), Dutton (1986), and Colin de Verdiere (1993).

Many authors cite Sandstrom's theorem because they believe the theorem is based on sound thermodynamic principles, and nobody wants to take the risk of violating the second law of thermodynamics. However, the application of Sandstrom's theorem to the oceanic circulation does pose a serious puzzle. The ocean is mostly heated and cooled from the upper surface. (Compared with other sources of energy, energy due to the geothermal heating is much smaller; however, its contribution to the oceanic general circulation may not be totally negligible, as will be discussed shortly.) Due to thermal expansion, the sea surface level at low latitudes where heating takes place is about one meter higher than the sea level at high latitudes where cooling takes place. Therefore, according to Sandstrom's theorem, there should be no convectively driven circulation. Thus, the existence of the strong meridional overturning circulation in the oceans, poses a serious challenge for Sandstrom's theorem.

Although the discrepancy between Sandstrom's theorem and the oceans has been known for many years, the problem remains unsettled. Many people have tried to find a mechanism that makes heating penetrate much deeper than cooling. This attempt has so far failed to yield satisfactory results because cooling-induced convection at high latitudes can easily penetrate to one kilometer below the surface, but it is hard to find a simple mechanism that makes heating penetrate even deeper.

The difficulty associated with Sandstrom's model is its highly ideal circulation physics, especially as it completely excludes diffusion and friction. As will be shown in this study, including diffusion will substantially change the model's behavior, and a detailed analysis of the dynamic balance in the model answers the questions posed by the old model. In section 2 we will begin with a detailed analysis of a simple tube model used by many investigators. The essential problem of Sandstrom's theorem is the lack of mixing in the model, so we will analyze the dynamic role of mixing in the tube model. In a stratified ocean, turbulent mixing requires mechanical energy. Using the scaling analysis we will derive a simple relation between the meridional overturning, poleward heat flux, and the energy source for mixing in the oceans. The energy sources for mixing in the oceans will be discussed in section 3, and the global-

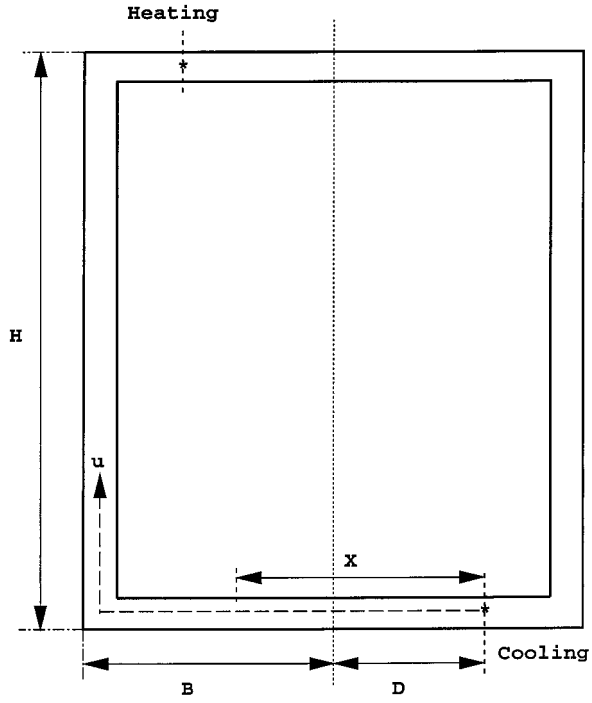

FIG. 2. An idealized tube model for the ocean.

mean mixing rate is estimated from energy budget analysis. The idea of fixed energy for mixing and the associated scaling law is tested using a primitive equation model, and many interesting results are discussed in section 4. Finally, the conclusions are summarized in section 5.

2. Mixing and mixing energy controlling the oceanic thermohaline circulation

a. Mixing-induced circulation in a tube model

Thermally driven circulation in the oceans can be idealized in terms of a tube model. The model consists of a closed square loop with two vertical arms of length H and two horizontal arms of length $2B$, Fig. 2. The tube has a uniform cross section of unit area, and temperature and velocity are assumed uniform across each section. The cooling source is located at a distance D from the origin (defined as the central point of the low arm) at the right-hand side of the lower arm, and the heating source is located at a directly opposite position at the left-hand side of the upper arm. When D is larger than B, the cooling source is located at a vertical level of $D - B$ in the right arm. When D is larger than $B + H$, the cooling source is located in the upper arm. Temperature at the cooling and the heating sources is maintained constant. In this study we will assume the fluid is Boussinesq so that heating/cooling do not change the volume of the fluid.

The density (temperature) distribution within the tube in a steady state is governed by a simple balance between density advection and diffusion,

$$u\rho_X = \kappa\rho_{XX}, \tag{2}$$

where X is the alongtube coordinate, defined positive clockwise from the cooling source. Introduce the following nondimensional numbers

$$s = \frac{X}{L}, \qquad b = \frac{B}{L}, \qquad d = \frac{D}{L}, \qquad h = \frac{H}{L},$$

$$L = 2B + H.$$

Assuming the circulation is steady and clockwise, the density distribution within the loop can be determined. We will label the solution to the left (right) of the cooling source with a superscript l (r),

$$\rho^l = \rho_2 - \Delta\rho R_1(e^{\alpha s} - 1), \tag{3}$$

$$\rho^r = \rho_2 - \Delta\rho R_2(e^{-\alpha s} - 1), \tag{4}$$

where ρ_2 is the density at the cooling source, $\Delta\rho = \rho_2 - \rho_1 > 0$ is the density difference, ρ_1 is the density at the heating source,

$$R_1 = (e^{\alpha} - 1)^{-1}, \qquad R_2 = (e^{-\alpha} - 1)^{-1},$$

$$\alpha = \frac{uL}{\kappa}. \tag{5}$$

In this study our focus is on the model's behavior within a parameter range pertinent to a simple vertical advection and diffusion balance in the oceans; thus, we will use the following parameters: $L = 1$ km, $b = 0.25$, $h = 0.5$, the velocity will be in units of 10^{-7} m s^{-1}.

In a steady state, pressure torque is balanced by friction

$$\int_s \rho\mathbf{g}\ \mathbf{ds} = -r\rho_o u, \tag{6}$$

where $\mathbf{g}$ is gravitation vector and r is the friction parameter.

The strength of the circulation strongly depends on the location of the cooling source, Fig. 3. The solutions for $d < 0.5$ (heating source is higher than cooling source) are shown in the left panel. Since mixing rate is normally less than 10^{-4} m^2 s^{-1}, only the left part of this panel is relevant to the oceans. For any given d, it is clear that the circulation is almost linearly proportional to the mixing rate κ, but it is insensitive to friction r. Thus, the circulation is mixing controlled and this case resembles the meridional circulation in the oceans.

To obtain a circulation on the order of 10^{-7} m s^{-1}, we need a mixing rate of 10^{-4} m^2 s^{-1}. When mixing is very weak, on the order of 10^{-7} m^2 s^{-1} (molecular diffusion), the nondimensional velocity will be on the order of 10^{-3} (or 10^{-10} m s^{-1} dimensionally). This is equivalent to 3-mm displacement per year, and it is probably very difficult to observe. Thus, both Sandstrom's observation and Jeffreys's argument are correct.

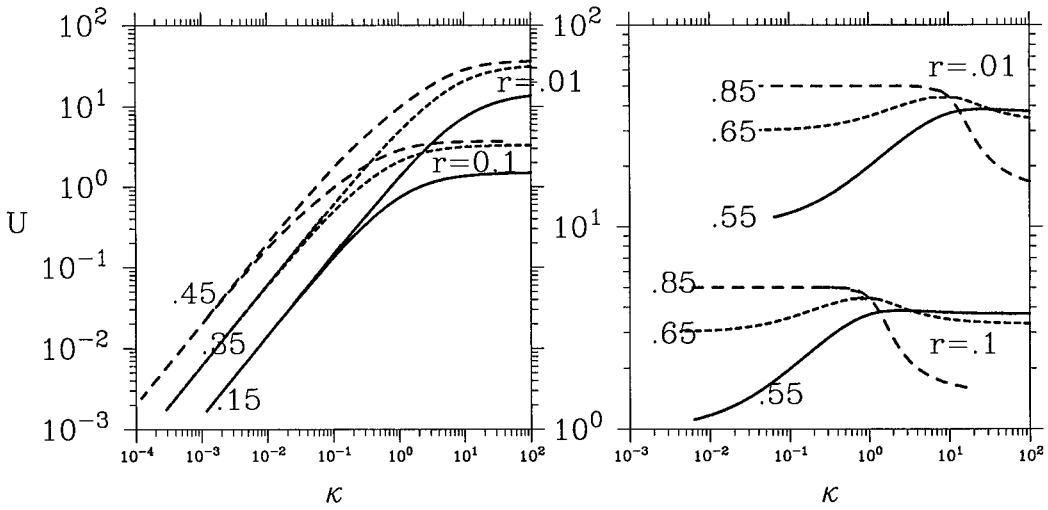

FIG. 3. Dependency of circulation rate (U in 10^{-7} m s^{-1}) on the mixing rate (κ in 10^{-4} m^2 s^{-1}). Numbers in the figures are the location d of the cooling source, and $r = 0.1$, 0.01 are values for the friction parameter.

The cases of $d > 0.5$ (cooling source is higher than the heating source) are shown in the right panel of Fig. 2. For a given d (the location of cooling source), the circulation is insensitive to the mixing rate. When κ changes 1000 times, the circulation rate changes only slightly. However, the circulation rate is very sensitive to the friction parameter r. As r increases ten times, the circulation rate also changes about ten times. Thus, the circulation is frictionally controlled when the cooling source is at a level higher than the heating source.

b. Potential energy source due to mixing

Gravitational potential energy is one of the most important forms of energy driving the oceanic circulation. In a turbulent and stratified ocean, small-scale mixing due to turbulent and internal waves can raise the center of mass. As a result, mixing in the oceans requires mechanical energy, which can come from the turbulent kinetic energy and other sources. The linkage between mixing and potential energy in the oceans can be shown in a simple case of a Boussinesq model with linear equation of state. The thermodynamic equation and the continuity equation are

$$\frac{\partial}{\partial t}\rho + \mathbf{u}\cdot\nabla\rho = \kappa\nabla^2\rho + \mathrm{CV}, \tag{7}$$

$$\nabla\cdot\mathbf{u} = 0, \tag{8}$$

where CV indicates the convective contribution, which cannot be parameterized in terms of a constant mixing rate. We will confine our discussion to an ocean of fixed volume V, without mass flux exchange with its environment.

The time rate of change of potential energy is

$$\frac{d}{dt}E_p = g\iiint_V z\frac{\partial\rho}{\partial t}\,dv = \Phi_S^p + \Phi_{\mathrm{ME}} - \Phi_{\mathrm{PK}} - \Phi_{\mathrm{CV}}^p, \tag{9}$$

where $\Phi_S^p = g\kappa\iint\rho_z H\,dx\,dy$ is the potential energy source due to surface heating/cooling (H is the sea surface level), $\Phi_{\mathrm{PK}} = -\iiint g\rho w\,dv$ is the rate of conversion from potential to kinetic energy, $\Phi_{\mathrm{ME}} = \kappa g\iiint\rho_z\,dv = \kappa g\iint(\rho_b - \rho_s)\,dx\,dy$ is the rate of potential energy increase due to mixing supported by the mechanical energy source, and ρ_b and ρ_s are density at the bottom and the upper surface.

Note that in the steady state surface thermal forcing cannot create potential energy $\Phi_s^p = g\kappa\iint\rho_z H\,dx\,dy = 0$. Therefore, the potential energy balance is reduced to (Huang 1998)

$$\frac{d}{dt}E_p = \Phi_{\mathrm{ME}} - \Phi_{\mathrm{PK}} - \Phi_{\mathrm{CV}}^p = 0. \tag{9a}$$

In the case of no wind stress input, the only source of potential energy is the mechanical energy supporting mixing, and this energy is used to sustain momentum dissipation (through the Φ_{PK} term) and convection.

In the stratified oceans the vertical eddy mixing rate κ can be related to the energy dissipation rate through

$$\kappa N^2 = a\varepsilon, \tag{10}$$

where

$$N^2 = -\frac{g}{\rho_o}\frac{\partial\rho}{\partial z}$$

is the buoyancy frequency, ε is energy dissipation rate, and $a \approx 0.176$ is an empirical coefficient (Osborn 1980). In the following discussion, the energy dissipation rate

ε and factor a will be combined into a mixing energy rate e.

The analysis above can be easily extended to the general case of a stratified turbulent ocean with a realistic equation of state. It can be shown that mixing in a stratified turbulent ocean requires a transfer of energy from turbulent kinetic energy to potential energy; see appendix A.

Since $\overline{\rho w g}$ is a reversible conversion between kinetic and potential energy and $\overline{p(\partial u_\alpha/\partial x_\alpha)}$ is a reversible conversion between kinetic and internal energy, the apparent ''dissipation'' rate of turbulent kinetic energy would be

$$\mathrm{AD} = -\overline{\rho' w'}\,\overline{g} - \overline{g'(\rho' w' + \rho' \overline{w} + \overline{\rho} w')} - \overline{\sigma_{\beta\alpha} \frac{\partial u_\beta}{\partial x_\alpha}}. \quad (11)$$

Note that the last term on the right-hand side is always negative and it represents the real dissipation due to molecular viscosity. The first term is negative and it represents the mechanical energy required for sustaining vertical mixing in a stratified ocean. The second term represents the energy conversion due to the time-dependent component of the gravity field. Therefore, the first and second terms represent conversion from kinetic energy to potential energy, so the decline in turbulent kinetic energy does not entirely become ''wasted'' heat. In fact, a small percentage of the turbulent kinetic energy ''dissipation,'' represented by the empirical coefficient a in (10), is actually transformed to the large-scale potential energy. As discussed in this study, this energy is the energy required to sustain mixing, and it is the most important dynamic factor controlling the meridional overturning rate.

c. Scaling laws governing the meridional circulation

Motions in the oceans are ultimately driven by energy from different sources; thus, it is interesting to explore how energy available for mixing actually controls the strength of circulation. Most scaling laws governing the meridional circulation are based on a fixed mixing rate. For the nonrotating case see, for example, Rossby (1965); for the rotating case see, for example, Bryan (1987). As a comparison, we have derived the scaling laws for the case with fixed energy supporting mixing; see appendix B.

Most importantly, scaling analysis indicates that the meridional mass flux and heat flux are linearly proportional to the energy density for mixing. Thus, the amount of energy available for supporting mixing is what really controls the strength of circulation, so more energy means stronger circulation.

The meridional heat flux can be rewritten as

$$H = \rho_o M c_p \Delta T = A_o E, \quad (12)$$

where

$$A_o = \frac{a c_p}{g \alpha D_o}$$

and $E = eL^2 D_o$ is the basin-integrated energy for mixing. This suggests that the thermohaline circulation in the oceans can be thought of as a heat conveyor belt with an amplification factor A_o. Note that the amplification factor depends on the depth of the basin only. Assuming the depth of the ocean is 4 km, $\alpha = 0.167 \times 10^{-3}\ \mathrm{K}^{-1}$, and $a = 0.176$, this gives an amplification factor of 107. For a shallow basin, A_o is even larger. Thus, a small amount of energy input for mixing can drive the oceanic heat conveyor belt that transports a much larger amount of heat energy poleward.

These scaling laws are derived under several assumptions discussed in appendix B. For example, the energy for mixing is assumed to be roughly a constant. In addition, it is assumed that the vertical density advection is balanced by vertical diffusion. These assumptions may not represent good approximations for the real oceans. For example, as will be shown shortly, the energy density level in the oceans decreases by several orders of magnitude from top to bottom, so the simple scaling laws derived above may be inaccurate. Nevertheless, these scaling laws shed insight to the physical mechanisms responsible for establishing the strong link between the mixing energy and the circulation.

3. Mixing energy sources and mixing rate

The connection between mixing energy and the oceanic circulation can be examined through diagnosing the balance of the available potential energy based on numerical experiments obtained from primitive equation models, as discussed by Huang (1998). The model is forced by the same relaxation condition on temperature imposed on the upper surface, and the only difference is that the vertical mixing rate is a specified constant, which varies from $10^{-5}\ \mathrm{m^2\ s^{-1}}$ to $10^{-4}\ \mathrm{m^2\ s^{-1}}$ and $10^{-3}\ \mathrm{m^2\ s^{-1}}$ in three experiments. The available potential energy (APE) of the model ocean is diagnosed using the exact definition, that is, $E_a = g \iiint \rho z\, dv - g \iiint \rho_r z_r\, dv$, where the subscript r indicates the reference state (defined as a state with minimum potential energy). When the model reaches a final equilibrium state, the sources and sinks of the APE are exactly balanced:

$$\frac{dE_a}{dt} = \Phi_{\mathrm{TF}} + \Phi_{\mathrm{ME}} - \Phi_{\mathrm{SVM}} - \Phi_{\mathrm{SHM}} - \Phi_{\mathrm{PK}} = 0, \quad (13)$$

where $\Phi_{\mathrm{TF}} = g \iint B\,(h_{m/2} - Z)\, dx\, dy$ is the APE sources due to thermal forcing (subtracting the loss due to convective mixing),

$$\Phi_{\mathrm{SVM}} = g\kappa_v \iiint \left(-\frac{dz_r}{d\rho}\right)\left(\frac{\partial \rho}{\partial z}\right)^2 dv,$$

and

TABLE 1. Energetics of a simple ocean model. All the energy flux densities are in mW m^{-2}; k: vertical mixing rate in 10^{-4} $m^2 s^{-1}$, MOR: meridional overturning rate in Sv; (10^6 $m^3 s^{-1}$), PHF: poleward heat flux in 10^{15} W, HFD: poleward heat flux density, Φ_{ME}: APE source due to mechanical energy sustaining mixing, Φ_{TF}: APE source due to thermal forcing, Φ_{PK}: conversion rate from APE to kinetic energy, Φ_{SVM}: APE sink due to vertical mixing, and Φ_{SHM}: APE sink due to horizontal mixing.

k	MOR	PHF	HFD	Φ_{ME}	Φ_{TF}	Φ_{PK}	Φ_{SVM}	Φ_{SHM}
0.1	1.68	0.099	2690	0.206	0.234	0.0073	0.196	0.239
1.0	9.1	0.362	9835	1.927	1.197	0.155	1.693	1.277
10	33.27	1.131	30729	15.17	15.06	2.668	12.70	12.58

$$\Phi_{\mathrm{SHM}} = g\kappa_h \iiint \left(-\frac{dz_r}{d\rho}\right)\left[\left(\frac{\partial\rho}{\partial x}\right)^2 + \left(\frac{\partial\rho}{\partial y}\right)^2\right] dv$$

are the APE sinks due to vertical and horizontal mixing in the reference state. The external mechanical energy that supports mixing contributes about 50% of the APE source (Table 1). Furthermore, under the same thermal boundary condition, it is the level of external mechanical energy available for mixing that actually controls the strength of the circulation. Even the APE generated by the thermal forcing is also controlled by the amount of energy available for mixing.

As an example, for $\kappa_T = 10^{-4}$ m^2 s^{-1} the external energy density required to sustain the basic stratification is 1.927 mW m^{-2}, whereas the APE generated by thermal forcing is smaller, 1.197 mW m^{-2}. The ''output'' of mechanical energy from the model ocean is the potential-to-kinetic-energy conversion rate of 0.155 mW m^{-2}. The real output of mechanical energy from the system should be $\Phi_{PK} - \Phi_{ME} = -1.772$ mW m^{-2}. If one defines the heat efficiency of the oceanic engine as the ratio of the mechanical energy output to poleward heat flux (the heat flux through the engine), the efficiency is about $-1.772/9835 \approx -0.02\%$. Since the nominal heat efficient of the oceanic engine is *negative*, the ocean circulation is really not a heat engine at all. It is better to call the thermohaline circulation a heat conveyor belt, which can transport heat and freshwater poleward under a constant supply of external mechanical energy for mixing.

Of course, there is a theoretical limit in which the ocean circulation does work like a heat engine, and it is an oceanic circulation driven by molecular diffusion only. Since molecular diffusion is on the order of 10^{-8}–10^{-7} m^2 s^{-1}, the corresponding meridional overturning rate would be on the order of 0.1 Sv (Sv $\equiv 10^6$ m^3 s^{-1}), equivalent to a vertical velocity of a few millimeters per year and there would be a very shallow and sharp thermocline (order of a few meters) in the upper ocean. Such an imaginary circulation is very difficult to simulate with the traditional oceanic circulation models. The extremely weak circulation driven by molecular diffusion alone is, of course, totally irrelevant to the real oceans. For the realistic parameter regime, the ocean is not a heat engine, and an external mechanical energy source is required to sustain the circulation.

Estimates of the amount of energy available for mixing in the oceans vary greatly, depending upon the methods used. Faller (1966) made an attempt to determine the source of energy for the oceanic circulation, including contributions from wind stress, thermal forcing, the hydrological cycle, tidal energy, and pressure variations. A detailed budget for kinetic energy flux from the atmosphere to the oceans is made by Lueck and Reid (1984), with an estimate of average downward atmospheric flux of kinetic energy of about 1.4 W m^{-2}, but only 2%–10% of the downward flux of kinetic energy actually enters the oceans. We will use the conservative estimate of 30 mW m^{-2}. Assuming this energy is dissipated over the upper kilometer of the ocean leads to an energy density of 3×10^{-5} W m^{-3}.

Using the scaling laws and assuming $L = 6000$ km, $f = 10^{-4}$ s^{-1}, $\Delta T = 10$°C, and $a = 0.2$, we obtain the following estimates

$$\kappa = 10^{-4}\ \mathrm{m^2\ s^{-1}}; \qquad W = 0.36 \times 10^{-6}\ \mathrm{m\ s^{-1}};$$
$$D = 278\ \mathrm{m}; \qquad M_m = 13\ \mathrm{Sv};$$
$$H_m = 0.54 \times 10^{15}\ \mathrm{W}. \tag{14}$$

The winds are one possible source of energy for mixing; however, most of the energy from the wind stress seems to be trapped within the mixed layer and does not penetrate much deeper than the first few hundred meters of the upper ocean. Another way to estimate the wind stress contribution is to calculate $\tau \cdot \mathbf{u}_{\mathrm{geo}}$, where $\mathbf{u}_{\mathrm{geo}}$ is the subsurface geostrophic velocity. Wunsch (1998) has estimated that the wind stress work over the global oceans is about 8.8×10^{11} W (with a global mean 2.8 mW m^{-2}), using both the satellite altimeter data and the results from a ¼-degree resolution numerical model. However, 70% of this energy input occurs south of 40°S; thus, the mean energy source is 1 mW m^{-2} north of 40°S, which is much smaller than the value of 30 mW m^{-2} estimated by Lueck and Reid (1984). Apparently, the wind-stress energy input on the geostrophic currents is too small to be a major energy source sustaining mixing. However, the Southern Ocean is one exception. Since 70% of the wind energy input occurs south of 40°S, the mean energy source is 10 mW m^{-2} south of 40°S, about 10 times stronger than that in the other oceans. As will be shown shortly, however, this is still much lower than the energy density required for sustaining the strong mixing in the Southern Ocean.

The energy input associated with the subsurface geostrophic currents seems a direct source of the large-scale kinetic energy. On the other hand, the contribution due

to the high-frequency component of the wind stress, surface waves, and currents may be a substantial part of the total energy input. Another possible role of wind stress is the creation of the bow-shaped thermocline in the subtropical gyre and the dome-shaped density structure in the subpolar gyre, which contributes to the structure of the meridional overturning. However, the interaction between the wind-driven circulation and the thermohaline circulation will not be our focus in this study. Wind stress can certainly contribute to sustain mixing in the subsurfacial ocean; but, the energy pathway and its magnitude are not very clear. Therefore, our discussion here will be concentrated on the dynamic role of mixing driven by an energy source due to tides and geothermal heating.

a. Tidal mixing

The other major source of external energy sustaining mixing in the ocean interior seems to come from tidal mixing. The total tidal dissipation rate can be inferred from astronomical observations, such as the telescopic observations of lunar occultation, solar longitude, or variations in satellite orbit elements. A recent comprehensive review of the related issues can be found in the paper by Kagan and Sundermann (1996) and Munk and Wunsch (1998), Morrison (1978) estimated the total tidal dissipation rate was about 3.17×10^{12} W. Recent estimate based on satellite altimeter data and global tidal models is about 3.5×10^{12} W (Munk and Wunsch 1998).

Tidal dissipation primarily goes to two sinks: barotropic tidal dissipation in shallow seas, about 1.7×10^{12} W according to Miller (1966). The other sink is through barotropic tidal dissipation near seamounts and ridges as well as internal tides. Early studies tended to underestimate this part of energy dissipation. For example, Bell (1975) estimated that the energy dissipation through internal tides was less than 10% of the total tidal dissipation. However, recent studies suggest that internal tides generated near steep bottom topography, such as midocean ridges, constitute a substantial part of the tidal dissipation. Sjoberg and Stigebrandt (1992) estimated the energy flux into internal tides to be about 1.3×10^{12} W, whereas Morozov (1995) estimated it to be 1.1×10^{12} W, which corresponds to an average strength of 3.21 mW m^{-2}. These estimates of baroclinic tidal dissipation rate seem too large. The most recent studies based on satellite data and tidal models indicate that tidal dissipation rate in the open ocean (near the ridges and seamounts, excluding the marginal seas) is about 0.9×10^{12} W, with 0.7×10^{12} W due to the barotropic tidal dissipation and 0.2×10^{12} W due to the baroclinic tidal dissipation (Munk and Wusch 1998). This corresponds to a energy dissipation rate of 2.63 mW m^{-2}.

Since the midocean ridges in both the Indian and the North Atlantic Ocean are very steep, the internal tidal dissipation rate there is larger. Morozov (1995) estimated that the total energy flux due to semidiurnal internal waves (tides) was 0.4×10^{12} W for the Atlantic, 0.4×10^{12} W for the Pacific, and 0.3×10^{12} W for the Indian Ocean. Thus, the mixing rate in the Indian Ocean and the North Atlantic Ocean is about 50%–100% stronger than in other parts of the world oceans [except for the Antarctic Circumpolar Current (ACC)]. In fact, Sjoberg and Stigebrandt (1992) estimated that the vertical mixing rate in the depth range of 800–2000 m in the North Atlantic Ocean was about $0.7–1.0 \times 10^{-4}$ m^2 s^{-1}, well above the level of mixing in other oceans, especially the Pacific.

In any case, tidal mixing (including internal waves due to tidal flow) may be the most important energy source driving the thermohaline circulation. Without tidal mixing, there would be virtually no stratification or motion in the deep ocean. For example, a large basin without midocean ridges, or an imaginary planet earth without the moon would have a dramatically different thermohaline circulation and climate.

b. Geothermal heating

Near the axis of the midocean ridge, heat is released to the deep ocean as the newly formed seafloor cools off. The heat flux rate declines as the seafloor ages. Far away from the ridge crest, the geothermal heat flux drops to the background level of about 46 mW m^{-2}. The potential energy generated from geothermal heating can be calculated as the following. Assuming that seawater is a Boussinesq fluid and its density is a linear function of temperature only that is, the effects of salinity and pressure on density are neglected, the potential energy generated by thermal forcing from the boundary is

$$\Phi_s = g \iint Bz \, dA, \tag{15}$$

where $B = (\overline{\rho}\alpha\dot{Q})/c_p$ is the buoyancy flux through the boundary, $\overline{\rho}$ is the mean density, $\alpha = 0.000\,167\ ^\circ\mathrm{C}^{-1}$ is the thermal expansion coefficient, c_p is the heat capacity under constant pressure, and $\dot{Q}$ is the heating rate.

Note that under the Boussinesq and the rigid-lid approximations, sea surface heating and cooling cannot generate potential energy (Huang 1998). On the other hand, although geothermal heating is about 50 times smaller than the heat flux associated with sea surface heating/cooling, it can create a substantial amount of potential energy because the ocean is heated at the bottom and cooled from the sea surface. Assume that the origin of the coordinates is located at the surface, the potential energy created by geothermal heating can be easily calculated

$$\Phi_s = g \iint Bh_b \, dA, \tag{15a}$$

where h_b is the bottom depth.

Geothermal heat flux through the ocean bottom is closely related to the age of the bottom rock. Near the axis of the midocean ridge, a large amount of heat is released through heat conduction and geothermal vents. As the newly formed bottom rocks move away from the axis of the ridge, the heat flux gradually declines. There have been several models specially designed to fit the observations. In this study we use the global depth and heat flow model by Stein and Stein (1992). According to their model, the age of the bottom rock can be calculated by

$$t = \sqrt{\frac{d - 2600}{3.65}}, \qquad \text{if } d \le 4291.7;$$
$$t = -\frac{\ln[(5651 - d)/2473.0]}{0.0278}, \quad \text{if } d \ge 4291.7, \qquad (16)$$

where d is the seafloor depth in meters, and t is age in units of Myr. The heat flux (in mW m^{-2}) is a function of age

$$\dot{Q} = \begin{cases} 510t^{-1/2} & \text{if } t \le 55 \\ 48 + 96e^{-0.0278t} & \text{if } t \ge 55. \end{cases} \qquad (17)$$

For depths greater than 5651 m, the heat flux rate is set to the constant rate of 48 mW m^{-2}.

Using the NOAA global ocean topography data with $1^\circ \times 1^\circ$ resolution, the total amount of potential energy generated by geothermal heating is calculated. For simplicity, the contribution due to bottom topography shallower than 2500 m is neglected because this is mostly the shallow continental margins, to which the geothermal heat flux formulas do not apply.

The global integrated geothermal heat flux is 32×10^{12} W (Stein and Stein 1992; Stein et al. 1995), with a mean flux rate of 87.8 mW m^{-2}. The total potential energy generated is 0.497×10^{12} W, with a mean rate of $\overline{e} = 1.37$ mW m^{-2}. If one uses the mean depth and mean flux rate, the energy generated would be 0.46×10^{12} W, very close to the value obtained by the more accurate calculation. The sum of the energy sources due to tidal mixing and geothermal heating is $2.63 + 1.37 = 4.00$ (mW m^{-2}). Note that the empirical formulas used here may be substantially modified as our knowledge about the geothermal heat flux improves. However, it is clear that geothermal heat flux is one of the most important contributors to the mechanical energy sustaining mixing in the deep ocean.

It is interesting to note that, according to formula (15a), the potential energy generated by geothermal heating is mostly due to the off-axis part of the seafloor. Although heat flux near the midocean ridge is quite large, its depth relative to the sea surface is small, so the rate of potential energy generation, Bh_b, is not necessarily much larger than that of the contribution due to the off-axis part where the depth difference is large, but the heat flux is relatively small. The global distribution of geothermal heat flux among the oceans is rather uniform. For example, the Atlantic basin average is about 1.34 mW m^{-2}, which is very close to the global mean.

The potential energy due to the geothermal heat flux contribution is about 55% of the tidal dissipation. This suggests that geothermal heating may play an important role in the global thermohaline circulation. However, much of this potential energy may be dissipated within the bottom boundary layer. So far, geothermal heating has been entirely neglected in oceanic general circulation models because geothermal heat flux is less than 2% of the surface heat flux. However, since the oceans are heated from below by the geothermal heat flux and cooled from above, this mode of thermal forcing is very efficient, as demonstrated by Sandstrom and many scientists afterward.

Thus, it may be very important to assess the dynamic role of geothermal heating in the global-scale thermohaline circulation. In fact, there have been many studies devoted to the special role of geothermal heating in driving circulation at middle and deep levels, (e.g., Joyce et al. 1986; Helfrich and Speer 1995). It would be very interesting to extend these studies to basin scales by imposing a geothermal heat flux condition at the base of the numerical model. The dynamic role of geothermal heat can be much more important for the abyssal circulation and deep water mass transformations, especially near a midocean ridge.

Although the amount of water through the venting of high temperature (350°C) is rather small, the total amount of seawater entrained by the geothermal vents can be enormous. Lupton et al. (1985) estimated that each calorie of hydrothermal heat should vertically transport 25 cm^3 of ambient seawater. Extrapolating this local estimate to the global midocean ridge yields a total volume flux of 12×10^6 m^3 s^{-1}. (Another way to estimate the vertical volume flux is to assume that the average temperature difference is one degree between the entrained water and the ambient water. The total amount of geothermal heat flux of 32×10^{12} W can heat up about 8 Sv of water.) Thus, the vertical mass flux induced by geothermal heat flux is comparable with the vertical mass flux associated with the global thermohaline circulation (Kadko et al. 1995).

Furthermore, geothermal heat flux in the earth's history varies greatly because of strong fluctuations in tectonic activity, especially the crustal accretion rates. For an example, the crustal accretion rates during the late Archean (3000–2700 Ma) were about 10 times faster than the present rates in the southwest Pacific, thus geothermal heat flux at that time was much larger than the present flux rate. Similarly, geothermal heat flux during the Cretaceous might be much larger than the present level. Kadko et al. (1995) gave a comprehensive review of the historic evolution of geothermal heating and its links with other components of the earth system. It is suggested that in the future the mixing rate used in paleocirculation models must be linked to the geother-

mal heat flux during the studied period in order to simulate the physics accurately.

c. Mixing rate inferred from mixing energy

Mixing raises the center of water masses, so mechanical energy is required for mixing. Mixing energy can be easily calculated for a Boussinesq fluid (e.g., Huang 1998). The situation in the oceans is much more complicated because of the nonlinearity of the equation of state, especially the density effect due to both pressure and salinity. Since we are only interested in an estimate of mixing energy, we will use the vertical gradient of potential density, and the mixing energy is thus defined as

$$\iint \kappa_\rho g(\rho_b^\theta - \rho_s)\, dx\, dy, \tag{18}$$

where κ_ρ is the vertical turbulent density mixing coefficient, ρ_b^θ is the potential density at the bottom, referred to the sea surface, and ρ_s is the surface density. Assuming $\kappa_\rho = 10^{-4}$ m^2 s^{-1} and $\overline{\rho_b^\theta - \rho_s} = 3$ kg m^{-3}, we obtain the basin mean energy required for mixing as 3 mW m^{-2}.

The major problem is the uncertainty of the mixing rate. To obtain an estimate of the basin-mean mixing rate, we use the energy balance

$$e_{\text{mix}} = 0.176(\varepsilon_{\text{tides}} + \varepsilon_{\text{geothermal}}) = \frac{1}{A}\iint \kappa_\rho g(\rho_b^\theta - \rho_s)\, dx\, dy, \tag{19}$$

where $e_{\text{mix}} = 0.703$ mW m^{-2} is the effective mixing energy due to tidal dissipation and geothermal heat flux. This is equivalent to a global effective mixing energy of $E_{\text{mix}} = 0.242 \times 10^{12}$ W. Using the Levitus (1994) data and the UNESCO equation of state, we have calculated that the basin-mean mixing rate is $\kappa_\rho = 0.222 \times 10^{-4}$ m^2 s^{-1}.

Similar results can be obtained for a Boussinesq ocean. Assuming a simple linear equation of state

$$\rho = \rho_0(-\alpha\Delta T + \beta\Delta S), \tag{20}$$

then the corresponding mixing rate inferred from the Levitus data is about 0.256×10^{-4} m^2 s^{-1}, which is only slightly larger than the value of 0.222×10^{-4} m^2 s^{-1} inferred from the potential density calculation.

The strength of mixing energy peaks near the equator and declines toward high latitudes (Fig. 4). There is a minimum near 65°N. The reason for low mixing energy density in this area is due to the fact that deep water is formed in the Norwegian and Greenland Seas, thus vertical stratification here is rather weak. Similarly, mixing energy calculated around the edge of Antarctica is also small. Since the distribution of geothermal heat flux and tidal dissipation may not have the same pattern as the mixing energy, there must be some mechanisms (turbulence and waves) in the oceans that can redistribute the mixing energy.

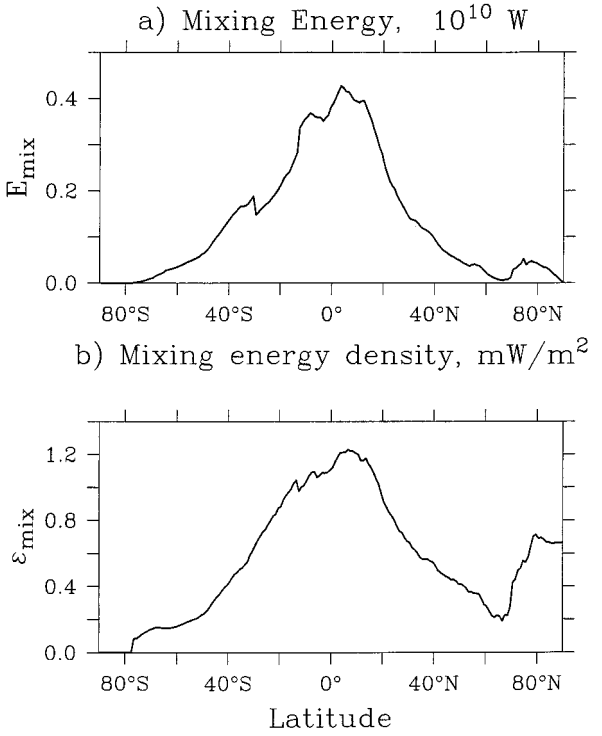

FIG. 4. (a) Meridional distribution of energy required for mixing, integrated over each 1° band, in 10^{10} W; (b) meridional distribution of energy density required for mixing, averaged over each 1° band, in mW m^{-2}.

The basin-mean mixing rate inferred from energy balance, 0.222×10^{-4} m^2 s^{-1}, is much smaller than the traditional value of 1.0×10^{-4} m^2 s^{-1}, first derived by Munk (1966) from global tracer balances, but it is still 2.5 times the value of 0.1×10^{-4} m^2 s^{-1}, inferred from many field observations carried out in the ocean interior, and the difference between these two values may be due to the strong bottom boundary mixing, say near the midocean ridge. Ledwell et al. (1993) carried out a tracer release experiment and estimated the diapycnal mixing rate to be 0.1–0.15 ($\times 10^{-4}$ m^2 s^{-1}) in the upper thermocline. Kunze and Sanford (1996) analyzed velocity profiles in the Sargasso Sea and obtained an average eddy diffusivity of 10^{-5} m^2 s^{-1}, independent of depth. However, recent field experiments have indicated that the diapycnal mixing rate is highly nonuniform in space (e.g., Toole et al. 1994; Polzin et al. 1997). In fact, the diapycnal mixing rate above the seafloor near the midocean ridge can reach 5×10^{-4} m^2 s^{-1}, which is 50 times larger than the values found by Ledwell et al. Given the strong mixing near the midocean ridge, a basin-mean mixing rate of 0.222×10^{-4} m^2 s^{-1} seems a reasonable estimate.

If energy input from the wind stress is included, the estimated diapycnal mixing rate increases. According to

the recent calculation by Wunsch (1998), north of 40°S, the mean energy flux due to wind stress is about 1 mW m^{-2}, so the corresponding mixing rate is increased to 0.278×10^{-4} m^2 s^{-1}. South of 40°S, energy input due to wind stress is about 10 mW m^{-2}; thus, the mixing rate is enhanced to a level of about 1.847×10^{-4} m^2 s^{-1}. This rate is substantially higher than that in the other oceans. However, there is evidence that suggest a much higher rate of mixing in the Southern Oceans. Using inverse methods, Olbers and Wenzel (1989) estimated that within the circumpolar current from 800 m to the bottom the vertical (diapycnal) mixing rate was about 10^{-3} m^2 s^{-1}. Recently, Polzin (1997, personal communication) analyzed Lowered Accoustic Doppler Current Profiler (LADCP) data collected in the Southern Oceans, and found that in several locations the vertical diffusivity below 1000 m was 4.4×10^{-4} m^2 s^{-1} or higher. Such strong mixing may be due to lee wave breaking generating by the strong current flowing over steep topography.

4. Numerical experiments based on fixed energy for mixing

Most oceanic general circulation models are based on the assumption of a fixed mixing rate. A very interesting and important question is how to parameterize mixing in climate-related models. Should we use the same mixing rate or same mixing energy when the climate is drifting? Clearly, fixing both mixing rate and mixing energy represent the two extremes, and the reality is likely to be between these two assumptions.

As discussed above, energy due to geothermal heating is a substantial part of the total energy available for mixing in the deep ocean, and this energy flux is independent of climate change. It is unclear how the tidal dissipation rate changes with climate change. Thus, a model with a fixed amount of energy for mixing may be a slightly better way to simulate climate change. In any case, since such a comparison has not been carried out, we decided to conduct experiments exploring the consequence of fixing mixing energy and to compare the results with that obtained from the common way of fixing the mixing rate.

There have been similar approaches used in oceanic circulation models. For example, a diapycnal mixing scheme based on specified mixing energy has been used in isopycnal models (Oberhuber 1993; McDougall and Dewar 1999). Other turbulent closure schemes, such as the Mellor and Yamada (1982) schemes and the Pacanofski and Philander (1981) scheme, have been commonly used. These schemes are based on the Richardson number or the turbulence kinetic energy, both calculated from the model. Although these schemes have been widely used for simulation of coastal circulation and equatorial circulation (mostly for the upper ocean), they may not be directly applicable to the large-scale thermohaline circulation. Because tidal dissipation and geothermal heating are the most important contributors for the mixing in the deep ocean, any mixing scheme excluding these factors cannot simulate the deep circulation correctly.

In this study, we will examine the behavior of a numerical model based on the idea of fixing the amount of energy available for mixing. In order to test this idea, the Bryan–Cox model (Bryan 1969; Cox 1984) is slightly modified. The model ocean has 25 layers of uniform thickness of 100 m, with a low horizontal resolution of $4° \times 4°$, extending from the equator to 60°N and 60° wide in the longitudinal direction. A complete convective adjustment scheme is used whenever the startification is unstable (Yin and Sarachik 1994). There is no wind stress or haline forcing, and the water density is a simple linear function of temperature

$$\rho = \rho_0(1 - \alpha T), \qquad \alpha = 0.000\,167\ ^\circ\mathrm{C}^{-1}. \quad (21)$$

The temperature balance obeys

$$\frac{\partial T}{\partial t} + (uT)_x + (vT)_y + (wT)_z = (\kappa_T T_z)_z + A_T(T_{xx} + T_{yy}). \quad (22)$$

In most traditional ocean circulation models, the rate of vertical tracer mixing, κ_t, is specified. As discussed above, we have formulated a model based on a fixed energy flux available for mixing; thus

$$e = g\alpha\kappa_T T_z \quad (23)$$

is specified, and the new temperature balance equation is

$$\frac{\partial T}{\partial t} + (uT)_x + (vT)_y + (wT)_z = \left(\frac{e}{g\alpha}\right)_z + A_T(T_{xx} + T_{yy}), \quad (24)$$

where $e = e(x, y, z)$ is the fixed external energy source for mixing.

As a major difference from most traditional models where the mixing rate is specified, the vertical diffusion rate in the new model varies with time; however, the total external energy supporting mixing is fixed instead. Several energy flux profiles have been tested (Fig. 5).

a. A linear energy profile

First, we choose a simple profile, labeled A in Fig. 5, which is linear in both y and z directions

$$e = \left(E_{\max} - (E_{\max} - E_{\min})\frac{h}{H}\right)\left(1 - \frac{y}{Y}\right), \quad (25)$$

where $E_{\max}$ ($E_{\min}$) is the maximum (minimum) energy flux at the surface (bottom) layer along the southern boundary. The energy flux is reduced to zero at the northern boundary because stratification there is very

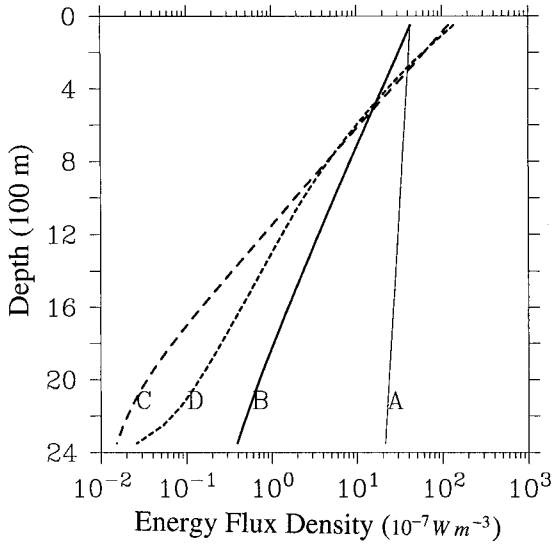

FIG. 5. Energy profiles used in the numerical experiments (only the profiles along the southern edge shown here). See the main text for the definitions of profiles A, B, C, and D.

weak, and the amount of energy required to support mixing there should be very small.

Using the linear profile we first carried out two sets of numerical experiments, A-1 and A-2, in which the energy flux profile is uniformly multiplied by a factor. The parameters of these experiments are listed in Table 2. Results from these experiments basically confirmed the simple scaling law discussed in appendix B. In fact, the meridional overturning rate and poleward heat flux are almost linearly proportional to the strength of the energy flux, Fig. 6.

In another set of experiments, A-3, we fixed the energy flux profile but changed the north–south reference temperature difference, Fig. 7. As predicted by the scaling law, the meridional overturning rate declines as the north–south temperature difference increases; however, the poleward heat flux remains almost unchanged. Thus, the scaling law seems valid for such a simple linear profile. The decline of meridional overturning rate due to the increase of the north–south temperature difference can be explained as follows. A large north–south temperature difference induces a strong stratification, which tends to suppress the vertical motion and leads to small meridional overturning rate.

TABLE 2. Parameters used in numerical experiments. A, B, C, and D are the energy profiles plotted in Fig. 5; A_m and A_T are the horizontal momentum and temperature diffusivity, κ_m and κ_T are the vertical momentum and temperature diffusivity, all in $m^2 s^{-1}$. The time step for velocity is 3 h and for the temperature, 2.5 days.

E-profile	A_m	A_T	κ_m	κ_T
A-1	500 000	500	0.0001	0.0001
A-2	500 000	1000	0.001	0.0001
A-3	500 000	200	0.001	0.0001
B	500 000	200	0.001	0.0001
C	500 000	200	0.001	0.0001
D	500 000	1000	0.0001	0.0001

b. An exponential energy profile

The oceanic energy source sustaining mixing is, of course, far from being a simple linear function of depth. Since the stratification decays exponentially with depth, an exponential profile seems more realistic. We have chosen an exponential profile

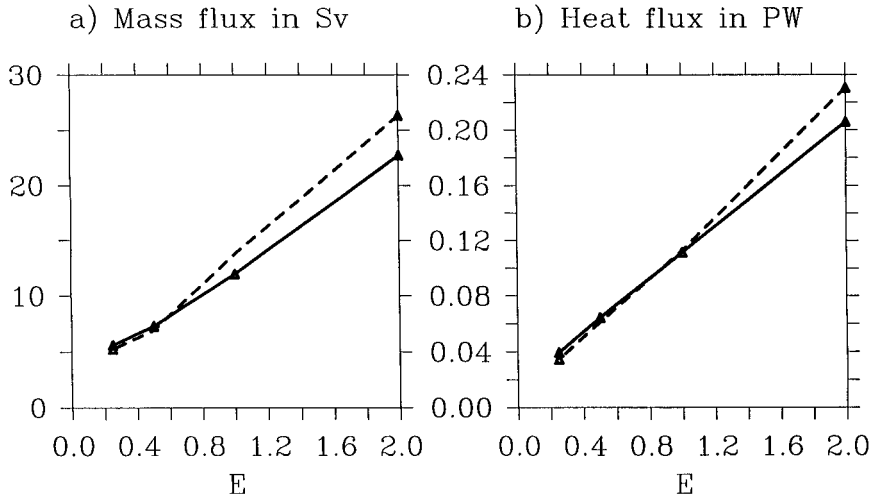

FIG. 6. Dependence of the meridional overturning rate (a) and poleward heat flux (b) on the strength of the external source of energy supporting mixing, based on a model with a linear profile of energy, profile A of Fig. 5. The horizontal temperature diffusivity is 500 $m^2 s^{-1}$ denoted by the solid lines, and 1000 $m^2 s^{-1}$ denoted by the dashed lines.

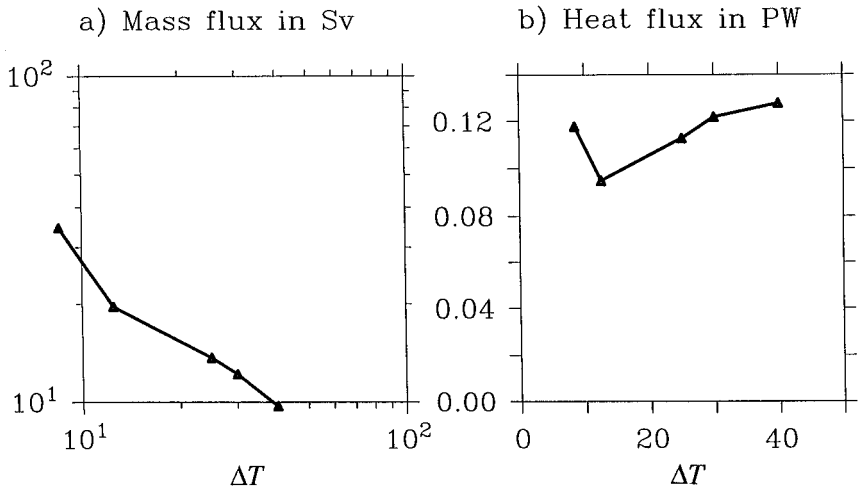

FIG. 7. Dependence of the meridional overturning rate (a) and poleward heat flux (b) on the north–south temperature difference, based on a model with a linear profile of energy, profile A of Fig. 5. Mass flux is in Sverdrups and heat flux in pentawatts (10^{15} W).

$$e = (E_{\min} + (E_{\max} - E_{\min})e^{-c(z/H)})\left(1 - \frac{y}{Y}\right), \quad (26)$$

where $c = 5$ for profile B and $c = 10$ for profile C.

Several sets of numerical experiments have been carried out by using this profile. Although the meridional circulation and poleward heat flux do increase roughly in proportion to changes in energy flux, the circulation rate under different north–south temperature differences does not follow the simple scaling law.

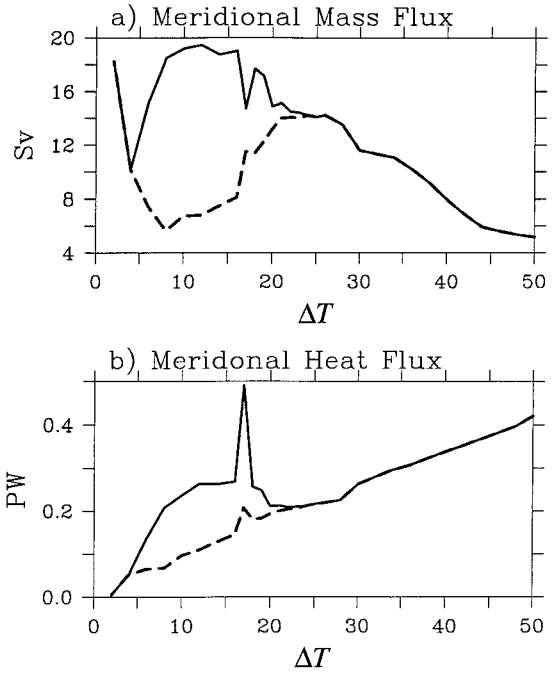

FIG. 8. Dependence of the meridional overturning rate (a) and poleward heat flux (b) on the north–south temperature difference, based on the model with an exponential profile of energy, profile B. Solid lines indicate the maximum and dashed lines indicate the minimum.

First, although the meridional overturning rate increases as the north–south temperature difference decreases, the model starts to oscillate when the temperature difference is smaller than 23°C. For a temperature difference smaller than such a value, the simple scaling law seems invalid. On the other hand, the poleward heat flux declines as the temperature difference is reduced, Fig. 8. For a very small temperature difference the poleward heat flux approaches zero.

The failure of the scaling law should not be a surprise at all. The scaling law has been derived based on several important assumptions, such as the energy flux density is roughly a constant and that there is a simple balance between the vertical thermal advection and vertical diffusion. In the present case, the energy flux density varies more than 100 times from the surface to the bottom, thus the model may behave differently from the simple scaling law.

One of the most unexpected phenomena is the decadal variability in the model. Although the amplitude of oscillations is small near the Hopf bifurcation point, both the oscillation amplitude in the meridional overturning rate and poleward heat flux can be quite large when the model is far away from the Hopf bifurcation boundary, Fig. 8.

In order to study such behavior we first run the model to a quasi-equilibrium under a given ΔT (In most cases the model is run for 1370 years.) Then the model is restarted from the existing equilibrium state and run under a slightly different ΔT. Since the difference in ΔT is quite small, each additional experiment is run for 685 years, which is enough for the solution to reach a new quasi-equilibrium. For cases of long period or chaotic

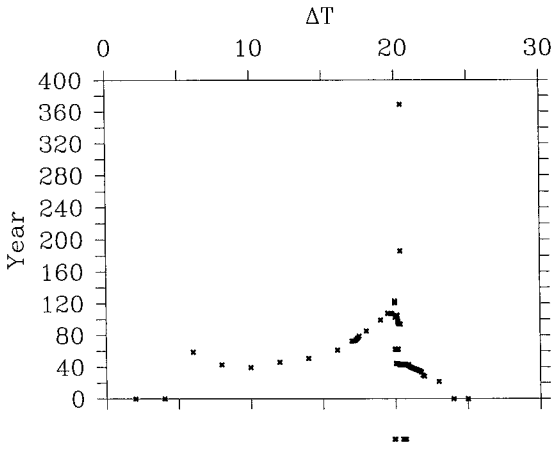

FIG. 9. Dependence of the oscillation period on the north–south temperature difference (using profile B of Fig. 5). Negative values indicate chaotic behavior.

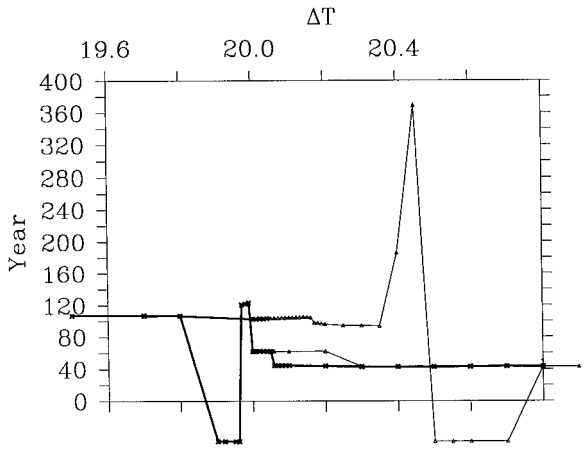

FIG. 10. Fine structure of the oscillation period road map, with negative values indicating chaotic behavior. The heavy line indicates the pathway when the north–south temperature difference is gradually reduced, and the thin lines indicate the pathways when the north–south temperature difference is gradually increased.

behavior, the model is run for a much longer time in order to obtain the right information about the periodicity or the chaotic behavior.

For the parameter region used in this set of experiments, the model enters the Hopf bifurcation for temperature difference smaller than 24°C (Fig. 9). In addition, multiple solutions, either stable limit cycle or chaotic solution, can exist for a certain parameter range, Fig. 10. For example, if ΔT is gradually reduced from 24°C, the system goes through a pathway depicted by the heavy line. At $\Delta T = 20.05$°C the period suddenly jumps from 44.4 to 62 yr. If the model is restarted from this new state, it tends to stay in the same state no matter whether ΔT is increased or reduced. As ΔT is reduced to 19.99°C, the period doubles. It seems that period quadrupling could be found, given enough fine searching. As ΔT is reduced to 19.97°C, the model enters a chaotic region. As ΔT is smaller than 19.80°C, the model falls back to a stable limit cycle, with a period of 107 yr.

On the other hand, if the model is restarted from such a stable limit cycle and ΔT is gradually increased, the model goes along a pathway depicted by the thin line in Fig. 10. At $\Delta T = 20.40$°C, the period doubles, and at $\Delta T = 20.45$°C, the period quadruples. For $\Delta T =$ 20.50–20.70°C, the model is in a chaotic state. Eventually, the model falls back to the simple stable limit cycle for $\Delta T > 20.80$°C.

Several cases demonstrating the typical time dependence of the solution are included, Fig. 11. For $\Delta T =$ 23°C, the model is restarted from a steady solution for $\Delta T = 24$°C. Clearly, the solution enters a limit cycle, and after 400 years the model reaches a stable limit cycle. The oscillation amplitude is rather small because it is very close to the Hopf bifurcation point. For smaller temperature difference, the limit cycle has a much larger amplitude, and for both $\Delta T = 19$°C and 20°C, the model is in a steady limit cycle after it is spun up from the previous solution. For $\Delta T = 20.60$°C, the model can have two possible states, one is a simple limit cycle with a period of 44 yr, the other is a chaotic state as shown in Fig. 11d.

Decadal variability in oceanic general circulation models has been discussed extensively; for a comprehensive review see Weaver and Houghes (1992). It is well known that low-resolution models under relaxation conditions for both temperature and salinity do not seem to have decadal variability. However, when the upper boundary conditions are changed to the mixed boundary conditions, that is, a relaxation condition for temperature and a flux condition for salinity, the decadal variability appears in the models (e.g., Weaver et al. 1991, 1993). Huang (1993) showed that a flux condition for the saline circulation alone can also produce decadal variability. Greatbatch and Zhang (1995) extended this idea and showed that a model with a fixed heat flux condition only can also have decadal variability, which apparently is rather similar to the decadal variability diagnosed from an ocean–atmosphere coupled model by Delworth et al. (1993). The appearance of decadal variability in oceanic circulation models is very closely related to the Hopf bifurcation. Using a simple loop model, Huang and Dewar (1996) demonstrated that replacing the relaxation condition with a flux condition can substantially lower the critical value of the Hopf bifurcation so that an oceanic model with a flux condition is well within the Hopf bifurcation region, and decadal variability is expected from models under such circumstances.

In the present case, although the model is under the relaxation condition on the upper surface, there is an energy flux condition for the interior grids. The new model behaves like the fixed diffusivity models under a flux boundary condition; thus, the model is very close

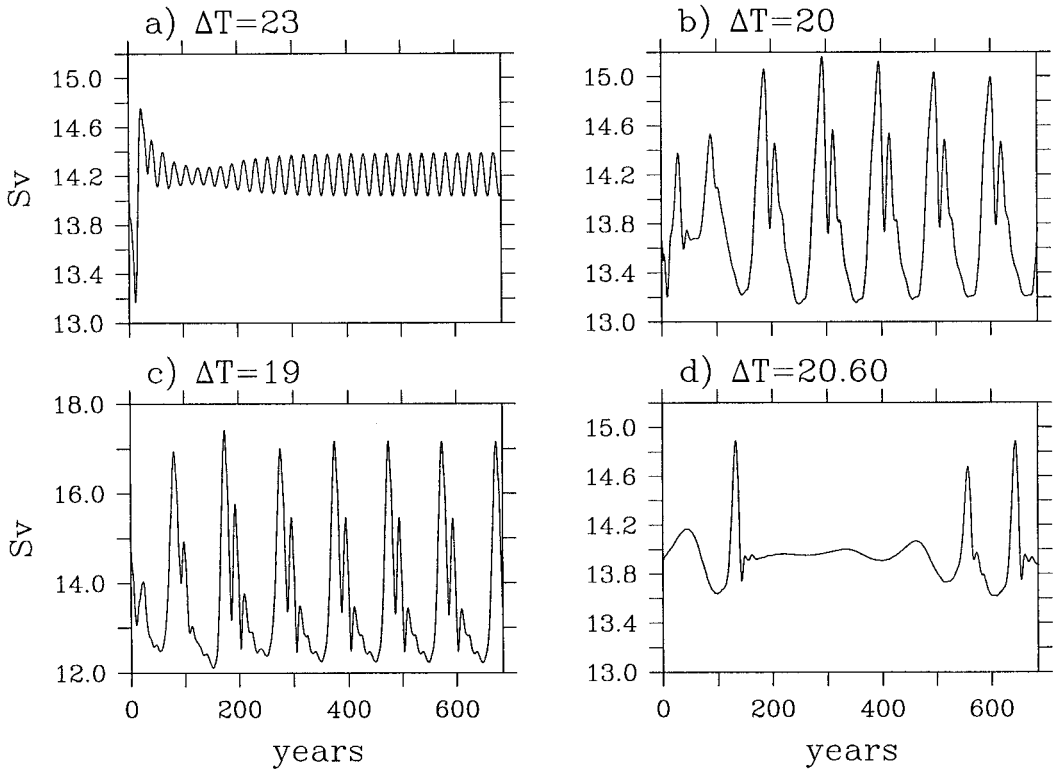

FIG. 11. Time dependence of the meridional overturning rate for different north–south temperature differences (profile B of Fig. 5): (a) $\Delta T = 23$°C, (b) $\Delta T = 20$°C, (c) $\Delta T = 19$°C, and (d) $\Delta T = 20.60$°C.

to or well within the Hopf bifurcation region, and decadal variability is expected. Decadal variability in our simple model suggests that oceanic models under a fixed energy source for mixing may have very rich decadal variability, and this has a very important dynamic meaning for climate study.

The mechanism for the decadal variability can be explained in terms of a meridional loop. The meridional overturning cell is ultimately driven by the meridional pressure difference. At the beginning of a cycle, the meridional overturning cell is slow, so heat transport is low; thus, the north–south temperature difference (here represented by the vertically and zonally averaged north–south temperature difference) increases. A positive meridional pressure gradient anomaly can induce a positive meridional overturning rate, which in turn induces a positive poleward heat flux. Such a relation is clearly shown by the 90° phase shift between the forcing and its consequence Fig. 12.

Winton (1996) explored the role of coast-trapped baroclinic currents in setting up the decadal variability in an oceanic general circulation model with fixed vertical mixing rate. Although the model based on a fixed amount of energy sustaining mixing may be different from the model with a fixed mixing rate, these coast-trapped baroclinic currents may play a similar role in the present case. However, exploration of the detailed mechanism for the decadal variability is left for further study.

c. Comparison with fixed mixing rate

In order to compare the new formulation of fixed energy for mixing with the old formulation of fixed mixing rate we have run three sets of experiments. First, we use an exponential energy profile with $a = 10$, the results are labeled as profile C, Fig. 5. Second, we run the old model (with fixed mixing rate) for the same configuration with $\kappa = 10^{-4}$ m^2 s^{-1}. After the model reaches its final equilibrium, the energy required to sustain mixing in the model is diagnosed and averaged along each latitude. The energy profile obtained also depends on the latitude, its vertical distribution along the southern rim of the basin is shown in Fig. 5 with label D. With profile D, we have carried out two sets of experiments to test the new model's sensitivity. In the first set we tested the model's sensitivity to the north–south reference temperature difference. In the second set we tested the model's sensitivity to changes in the energy flux profile.

The results from the first set of experiments are shown in Fig. 13. Since profile D is diagnosed from the model run with $\Delta T = 25$°C and $\kappa = 10^{-4}$ m^2 s^{-1}, the dashed line and the heavy line cross in the vicinity of $\Delta T =$

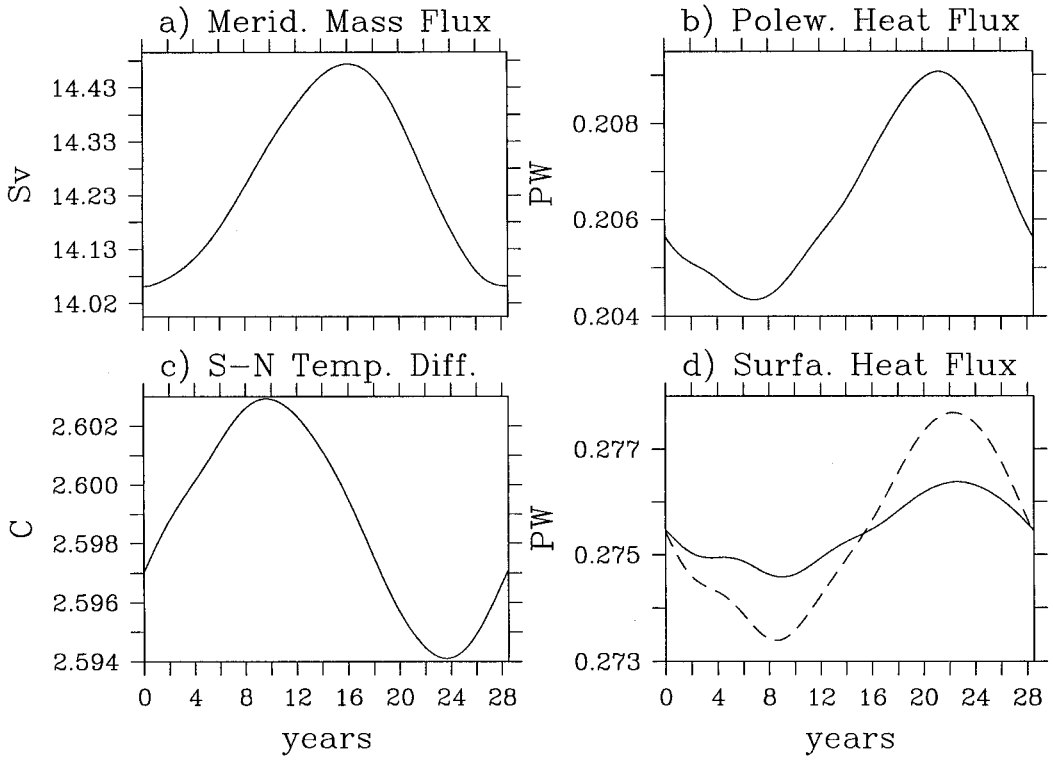

FIG. 12. Phase relation between different components of the circulation within one limit cycle for the case with ΔT = 22°C (profile B, Fig. 5). (a) Meridional overturning rate, in Sv; (b) poleward heat flux, in 10^{15} W, (c) vertically and zonally averaged north–south temperature difference (in °C); (d) surface heat flux, solid line for heat flux into the ocean and the dashed line for heat flux released from the ocean, in 10^{15} W.

25°C. However, the model with fixed energy is much less sensitive to climate changes. For example, as ΔT is reduced to 12.5°C, the meridional overturning rate and poleward heat flux are reduced to 12.7 Sv and 0.158 PW for the model with fixed mixing rate; however, the corresponding values are 15.4 Sv and 0.28 PW for the model with fixed energy.

Using a least squares fit, the power law for the case of fixed mixing rate is

$$M = 3.17 \times \Delta T^{0.552}, \quad H = 0.003\,98 \times \Delta T^{1.43}. \quad (27)$$

Thus, the Meridional mass flux increases in proportion to the 1/2 power law, similar to the case for the 1/2 power law when κ varies (Huang and Chou 1994). The poleward heat flux is close to the 4/3 power law obtained from the scaling analysis.

The least squares fitting gives the power laws for profiles C and D as

$$M_C = 7.09 \times \Delta T^{0.162}, \qquad H_C = 0.0332 \times \Delta T^{0.856} \quad (28)$$

$$M_D = 7.18 \times \Delta T^{0.287}, \qquad H_D = 0.0182 \times \Delta T^{0.888}. \quad (29)$$

Compared to the model with fixed mixing rate, the model with fixed energy (for both profiles C and D) is much less sensitive to climate changes.

The results from our numerical experiments may have important implications for climate studies. It is well known that the north–south temperature difference declines in a typical global warming scenario. Under such climate changes, the traditional models based on fixed mixing rate tend to predict a meridional overturning rate and poleward heat flux that are probably too small. From the energy argument, the oceans have a constant supply of tidal dissipation energy and geothermal heat flux, so the circulation tries to maintain its strength. Thus, within the regime of steady circulation (no decadal oscillations), a model with fixed energy flux for mixing is much less sensitive to climate changes. It is speculated that a coupled model based on fixed energy density may predict different climate variability under the same external forcing conditions.

In the second set of experiments we have also carried out three subsets of experiments to test the model's sensitivity to changes of the energy profile D. First, profile D is multiplied by a factor that is vertically constant; this will be called the standard case. Second, profile D is multiplied by a factor, which is one on the bottom (no change) and linearly increased (decreased) toward a specified factor on the surface; this will be called the surface-confined case. Third, profile D is multiplied by a factor, which is one on the surface and linearly increased (decreased) toward a specified factor on the bottom; this will be called the bottom-confined case. The

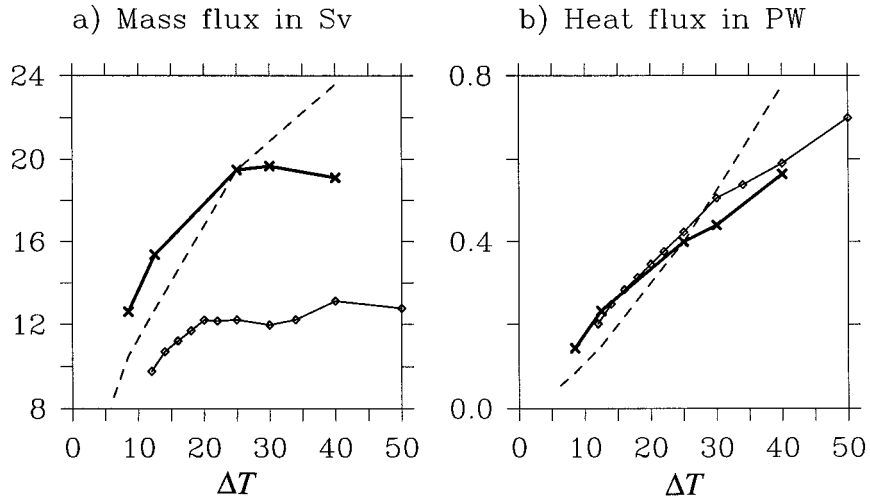

FIG. 13. Model's sensitivity to north–south temperature changes, (a) meridional overturning rate, (b) poleward heat flux. Dashed line indicated results from a model with fixed mixing rate of 10^{-4} m^2 s^{-1}, heavy line indicated results based on profile D, and thin line marked with small diamonds indicated results based on profile C.

profiles of basin-mean stratification resulting from such experiments are shown in Fig. 14.

Since energy flux declines with depth exponentially, the total energy change for the surface-confined case is very close to that of the standard case, but that for the bottom-confined case is quite different, Fig. 15a. Interestingly, the meridional overturning rate changes in response to an increase of energy for both the surface-confined and bottom-confined cases are about the same, and it is smaller than that of the standard case, Fig. 15b.

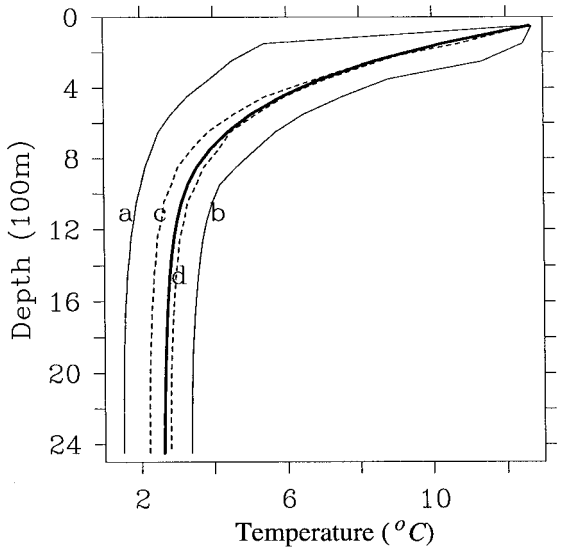

FIG. 14. Basin-mean temperature profiles based on energy profile D of Fig. 5. Solid line is for the standard case, thin solid lines are cases with surface-confined change in energy with line a for reduced to ½ and line b for increased twice; dashed lines are for cases of bottom-confined changes, line c for reduced to ½ and line d for increased twice.

However, when the energy flux density is reduced, the change in the meridional overturning rate is similar for the standard case and the surface-confined case; whereas changes for the bottom-confined cases are much smaller.

On the other hand, changes in the poleward heat flux are about the same for the standard case and the surface-confined case, but the poleward heat flux remains almost unchanged for the bottom-confined cases, Fig. 15d. The poleward heat flux is primarily controlled by the temperature structure within the upper ocean. When the mixing energy change is basically confined to the deeper part of the ocean, the deep temperature can change noticeably (as seen by the basin-mean temperature in Fig. 15c), but the surface temperature changes are small. As a result, poleward heat flux remains almost unchanged.

5. Conclusions

Using a loop model as an idealization of the oceanic thermohaline circulation, it is found that the circulation can be classified into two types, depending on the vertical locations of the heating and cooling sources. When the cooling source is at a level lower than the heating source, the circulation is mixing controlled and the rate of thermal circulation is primarily controlled by the amount of external energy available for mixing. Without external energy sources to support mixing, the mixing rate would be at a very low level determined by molecular diffusion. As a result, there would be no detectable thermal circulation, consistent with Sandstrom's theorem. However, if there is a strong external energy source, such as wind stress stirring and tidal dissipation in the ocean or mixing generated by some mechanical device in laboratory experiments, there can be strong thermal circulation, even if the cooling source is at the bottom of the tube.

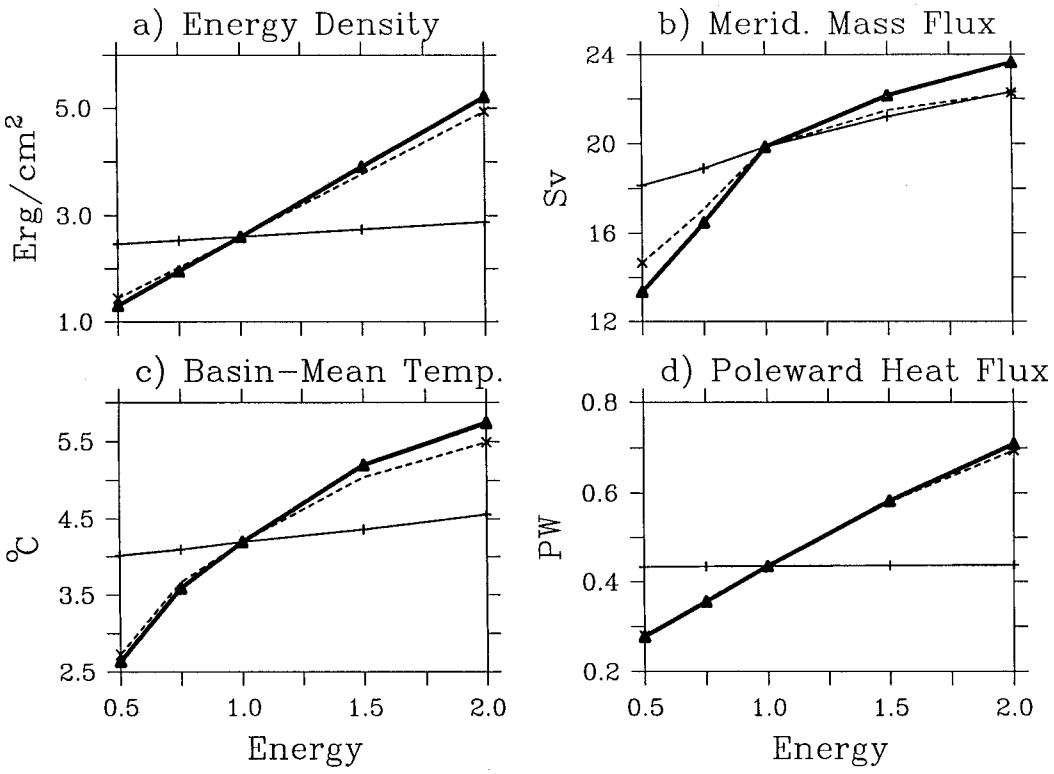

FIG. 15. Changes of the circulation in response to changes in the energy profile D of Fig. 5, heavy line indicates the standard cases, thin solid line for the cases of bottom-confined change, and the dashed line for the cases of surface-confined changes.

On the other hand, if the cooling source is at a level higher than the heating source, the circulation is friction controlled, and the amount of external energy available for mixing is unimportant. Since the atmosphere is heated primarily from the lower surface and cooled from above, its dynamics shares some similarity with the friction-controlled circulation in the loop model.

As a dramatic departure from the old paradigm that the rate of mixing is fixed, we have reexamined the question of what really controls the meridional circulation by assuming that the amount of energy available for mixing is fixed. In reality, the amount of energy for mixing may be linked to the stratification and the circulation itself, especially the energy dissipation associated with internal waves. However, it seems a good approximation to assume that mixing energy due to wind stress and tides is independent of the thermohaline circulation. Thus, we have made the assumption of fixing the amount of energy for mixing and explored its logical consequences.

A simple scaling analysis indicates that the meridional mass and heat fluxes are linearly proportional to the energy density available for mixing. Thus, energy supporting mixing in the ocean plays a fundamental role in controlling the strength of the meridional overturning rate and poleward heat flux. This raises many interesting questions about mixing, such as where does the energy come from, where does mixing take place, and what controls the mixing rate. In other words, a look at the same old questions from the point of view of energetics may actually help us to understand the oceanic circulation dynamics better.

Simple scaling does have limitations; thus, we have tested the sensitivity of a numerical model to the energy available for mixing. Although results from a simple energy profile seem consistent with the scaling laws, results from more realistic energy profiles showed that the simple scaling laws may not be accurate. Among other phenomena, the decadal variability of the model is very interesting and may have important applications to the decadal variability observed in the oceans.

Most interestingly, a model with fixed energy can respond to climate changes in ways quite different from the models with a fixed mixing rate. First, the model based on fixed energy at each grid point may be very close to the regime of decadal oscillation. This short-term variability of the model may be directly linked to the fact that the vertical diffusion term is now replaced with an energy source term. Second, within the regime of steady circulation, a model based on a fixed amount of energy available for mixing is much less sensitive to climate changes, compared with the traditional models that have a fixed mixing rate. Many existing numerical models treat the mixing rate as a fixed parameter; how-

ever, under different climate conditions the mixing rate might vary greatly. In fact, a certain amount of mechanical energy is needed to sustain mixing and thus the stratification and the circulation. Instead of assuming the mixing rate be fixed all the time, a numerical modeler should check how much mechanical energy is needed to support the model's circulation. The most important question one should ask is whether this amount of mechanical energy is really available.

A rather surprising result of this study is that geothermal heating can contribute a substantial portion of the energy for mixing of deep water. It should be very interesting to run some numerical experiments to explore the global dynamic effects of geothermal heating. Since a major portion of the potential energy generated from the geothermal heating may be lost within the bottom boundary layer, resolving such a boundary layer is critically important for such numerical experiments.

Based on the tidal energy and geothermal heat flux, the basin-mean estimate of the diapycnal mixing rate is about 0.22–0.28 ($\times 10^{-4}$ m^2 s^{-1}). Our estimate is much smaller than the classic value of 10^{-4} m^2 s^{-1} but is closer to the estimates from recent field observations.

At this time it is not clear how the mechanical energy available for mixing, such as tidal dissipation, internal waves, turbulence driven by wind stress stirring, and other sources, will change under different climate conditions. Thus, we have tested the model with the simplest possible assumption that the energy available for mixing is constant under climate changes. At this stage, our understanding of the mixing in the oceans remains preliminary at best. Although most numerical models are based on a fixed rate of mixing, there are observations that indicate that the mixing rate in the oceans changes with time. For example, Loder and Garrett (1978) found evidence for variable mixing in shallow water due to the 18.6-yr model tide and sea surface temperature variability associated with such a variable tidal mixing rate. Royer (1993) discussed oceanic variability in the northern North Pacific associated with the 18.6-yr tidal cycle. Thus, it would be interesting to run numerical models in which the mixing rate varies in both time and space according to the consideration of energy. In the future it may be necessary to study models in which mixing energy is, at least partially, controlled by stratification and circulation.

Acknowledgments. I have benefited from several interesting conversations with Dr. Carl Wunsch, who raised the issue about the oceanic heat engine and brought many classic papers to my attention. Dr. Ray Schmitt provided many useful comments. Reviewers comments helped me to improve the presentation greatly. I was supported by the National Aeronautics and Space Administration through Grant NAGW-4331 and by the National Science Foundation through Grant OCE96-16950.

APPENDIX A

Energy Balance for a Turbulent Ocean

In the following analysis we use some standard tensor notations, such as using α and β as dummy variables for summation. The overbar indicates ensemble average, and primes indicate perturbations. The basic equations are

$$\frac{\partial \rho}{\partial t} + \frac{\partial}{\partial x_\alpha}(\rho u_\alpha) = 0 \qquad \text{(A1)}$$

$$\frac{\partial u_i}{\partial t} + u_\alpha \frac{\partial u_i}{\partial x_\alpha} + \frac{1}{\rho}\frac{\partial}{\partial x_\alpha}(p\delta_{i\alpha} - \sigma_{i\alpha}) = X_i, \qquad \text{(A2)}$$

where

$$\alpha_{ij} = \mu\left(\frac{\partial u_i}{\partial x_j} + \frac{\partial u_j}{\partial x_i} - \frac{2}{3}\frac{\partial u_\alpha}{\partial x_\alpha}\delta_{ij}\right) + \mu'\frac{\partial u_\alpha}{\partial x_\alpha}\delta_{ij} \qquad \text{(A3)}$$

is the general viscous stress tensor,

$$X_i = -\frac{\partial \Phi}{\partial x_i} \qquad \text{(A4)}$$

is the external force (such as the gravity), and Φ is the potential.

The time evolution equation for the mean turbulent kinetic energy is (Monin and Yaglom 1971)

$$\frac{\partial \overline{K}}{\partial t} + \frac{\partial}{\partial x_\alpha}\Bigg[\overline{K}\,\overline{u}_\alpha + \overline{\rho}\,\overline{u}_\beta\overline{u'_\alpha u'_\beta} + \frac{1}{2}\overline{u}_\beta\overline{u}_\beta\overline{\rho' u'_\alpha} + \overline{u}_\beta\overline{\rho' u'_\beta u'_\alpha} + \frac{1}{2}\overline{(\overline{\rho} + \rho')u'_\beta u'_\beta u'_\alpha} + \overline{pu_\alpha} - \overline{u_\beta \sigma_{\beta\alpha}}\Bigg] = \overline{\rho u_\alpha X_\alpha} + \overline{p\frac{\partial u_\alpha}{\partial x_\alpha}} - \overline{\sigma_{\beta\alpha}\frac{\partial u_\beta}{\partial x_\alpha}}, \qquad \text{(A5)}$$

where $\overline{K} = \frac{1}{2}\overline{\rho u_\alpha u_\alpha}$ is the mean kinetic energy, $\overline{\rho u_\alpha X_\alpha}$ is the rate of potential and kinetic energy conversion, $p(\overline{\partial u_\alpha/\partial x_\alpha})$ is the rate of kinetic and internal energy conversion, and $\sigma_{\beta\alpha}(\overline{\partial u_\beta/\partial x_\alpha})$ is the rate of dissipation due to viscosity.

The time evolution equation for the internal energy e in a laminar ocean is (Fofonoff 1992)

$$\frac{\partial \rho_e}{\partial t} + \frac{\partial \rho u_\alpha e}{\partial x_\alpha} = -p\frac{\partial u_\alpha}{\partial x_\alpha} + \sigma_{\beta\alpha}\frac{\partial u_\beta}{\partial x_\alpha} - \frac{\partial F_\alpha}{\partial x_\alpha}, \qquad \text{(A6)}$$

where F_α is the internal energy flux. Taking the ensemble average, we have

$$\frac{\partial \overline{\rho e}}{\partial t} + \frac{\partial \overline{\rho u_\alpha e}}{\partial x_\alpha} = -\overline{p\frac{\partial u_\alpha}{\partial x_\alpha}} + \overline{\sigma_{\beta\alpha}\frac{\partial u_\beta}{\partial x_\alpha}} - \frac{\partial \overline{F_\alpha}}{\partial x_\alpha}. \qquad \text{(A7)}$$

The time evolution equation for the mean gravitational potential energy can be obtained by multiplying (A1) by Φ and taking the ensemble averaging

$$\frac{\partial \overline{\rho\Phi}}{\partial t} + \frac{\partial \overline{\rho u_\alpha \Phi}}{\partial x_\alpha} = -\overline{\rho u_\alpha X_\alpha} + \overline{\rho\frac{\partial \Phi}{\partial t}}, \qquad \text{(A8)}$$

where $\rho(\overline{\partial\Phi/\partial t})$ represents the energy source due to the time-variable component of the gravitational force, such as the tidal forces. Since the energy exchange between the potential, internal, and kinetic energy balance equations exactly cancel each other, this term represents a net contribution to the total energy budget. The other types of energy source come into play through the surface stress term in the turbulent kinetic energy balance and the internal energy flux term in the internal energy balance.

Thus, in a turbulent ocean the conversion from kinetic to potential energy is represented by a term $-\overline{\rho u_\alpha X_\alpha}$, or $\overline{\rho w g}$ in local Cartesian coordinates. This exchange term can be separated into several terms

$$\overline{\rho w g} = \overline{\rho}\,\overline{w}\,\overline{g} + \overline{\rho' w'}\,\overline{g} + \overline{g'(\rho' w' + \rho' \overline{w} + \overline{\rho} w')}. \quad \text{(A9)}$$

The first term on the right-hand side represents the kinetic to potential energy conversion associated with the ensemble mean density and velocity fields. The second term on the right-hand side represents the contribution due to turbulent mixing. In a stratified fluid, upward motion is usually correlated with positive density anomaly, so turbulent mixing in a stratified ocean requires a positive conversion from kinetic to potential energy.

The remainder of the terms on the right-hand side represent the potential to kinetic energy conversion due to the time-dependent component of the gravitational force, such as the tidal forces. Clearly, a mixing parameterization excluding tidal mixing is incomplete.

APPENDIX B

Scaling Laws for the Meridional Overturning Rate

Our study is confined to a model ocean forced by a temperature relaxation condition at the upper surface. Assuming the mixing energy is fixed, (10) can be rewritten as

$$\kappa g' = eD, \qquad g' = g\alpha\Delta T. \quad \text{(B1)}$$

where D is the scale depth, ΔT is the north–south temperature difference. Under a strong relaxation condition, ΔT is approximately the same as ΔT^*, the north–south reference temperature difference. Assume the heat balance in the main thermocline is between vertical advection and diffusion

$$W = \frac{\kappa}{D}. \quad \text{(B2)}$$

The vertical velocity scale is

$$W = \frac{e}{g'}. \quad \text{(B3)}$$

Thus, the meridional mass and heat fluxes are

$$M = WL^2 = \frac{L^2 e}{g'}, \quad \text{(B4)}$$

$$H = \rho_o c_p \Delta T M = \frac{\rho_o c_p L^2}{g\alpha} e. \quad \text{(B5)}$$

Using the scaling for the continuity and thermal wind relation

$$UD = WL, \qquad g'D = fUL \quad \text{(B6)}$$

and eliminating U, the scale depth can be obtained and the scale of U and κ can be derived accordingly. For the case of nonrotation

$$D = LE_n^{-1/4}, \qquad U = \frac{e}{g'}E_n^{1/4},$$
$$\kappa = \frac{Le}{g'}E_n^{-1/4}, \qquad E_n = \frac{g'^2 L^2}{\nu e}. \quad \text{(B7)}$$

For the case with rotation

$$D = LE_f^{-1/2}, \qquad U = \frac{e}{g'}E_f^{1/2} = \sqrt{\frac{e}{f}},$$
$$\kappa = \frac{Le}{g'}E_f^{-1/2}, \qquad E_f = \frac{g'^2}{fe}. \quad \text{(B8)}$$

Most importantly, these scaling laws indicate that meridional overturning rate and poleward heat flux is directly controlled by the amount of energy sustaining mixing.

REFERENCES

Bell, T. H., 1975: Topographically generated internal waves in the ocean ocean. *J. Geophys. Res.*, **80,** 320–327.

Bryan, K., 1969: A numerical method for the study of the circulation of the world ocean. *J. Comput. Phys.*, **4,** 347–376

——, 1987: Parameter sensitivity of primitive equation ocean general circulation models. *J. Phys. Oceanogr.*, **17,** 970–985.

Colin de Verdiere, A., 1993: On the oceanic thermohaline circulation. *Modelling Oceanic Climate Interactions,* J. Willebrand and D. L. T. Anderson, Eds., D. Reidel, 151–183.

Cox, M. D., 1984: A primitive equation, 3-dimensional model of the ocean. GFDL Ocean Group Tech. Rep. 1, GFDL/Princeton University, 141 pp.

Defant, A., 1961: *Physical Oceanography.* Vol. 1. Pergamon, 728 pp.

Delworth, T., S. Manabe, and R. J. Stouffer, 1993: Interdecadal variations of the thermohaline circulation in a coupled ocean–atmosphere model. *J. Climate,* **6,** 1993–2011.

Dutton, J., 1986: *Dynamics of Atmospheric Motion.* Dover, 617 pp.

Faller, A., 1966: Sources of energy for the ocean circulation and a theory of the mixed layer. *Proc. Fifth U.S. National Congress of Applied Mechanics,* Minneapolis, MN, American Society of Mechanical Engineers, 651–672.

Fofonoff, N. P., 1992: Lecture Notes EPP-226, Harvard University, 60 pp.

Greatbatch, R. J., and S. Zhang, 1995: An interdecadal oscillation in an idealized basin forced by constant heat flux. *J. Climate,* **8,** 81–91.

Helfrich, K. R., and K. G. Speer, 1995: Oceanic hydrothermal circulation: Mesoscale and basin-scale flow. *Seafloor Hydrothermal Systems: Physical, Chemical, Biological, and Geological Inter-*

actions, Geophys. Monogr., No. 91, Amer. Geophys. Union, 347–356.
Hodske, C. L., T. Bergeron, J. Bjerknes, and R. C. Bundgaard, 1957: *Dynamic Meteorology and Weather Forecasting.* Amer. Meteor. Soc., 800 pp.
Huang, R. X., 1993: Real freshwater flux as a natural boundary condition for the salinity balance and thermohaline circulation forced by evaporation and precipitation. *J. Phys. Oceanogr.,* **23,** 2428–2446.
——, 1998: On available potential energy in a Boussinesq ocean. *J. Phys. Oceanogr.,* **28,** 669–678.
——, and R. L. Chou, 1994: Parameter sensitivity study of the saline circulation. *Climate Dyn.,* **9,** 391–409.
——, and W. K. Dewar, 1996: Haline circulation: Bifurcation and chaos. *J. Phys. Oceanogr.,* **26,** 2093–2106.
Jeffreys, H., 1925: On fluid motions produced by differences of temperature and humidity. *Quart. J. Roy. Meteor. Soc.,* **51,** 347–356.
Joyce, T. M., B. A. Warren, and L. D. Talley, 1986: The geothermal heating of the abyssal subartic Pacific Ocean. *Deep-Sea Res.,* **33,** 1003–1015.
Kadko, D., J. Baross, and J. Alt, 1995: The magnitude and global implications of geothermal flux. *Seafloor Hydrothermal Systems: Physical, Chemical, Biological, and Geological Interactions, Geophys. Monogr.,* No. 91, Amer. Geophys. Union, 446–466.
Kagan, B. A., and J. Sundermann, 1996: Dissipation of tidal energy, paleotides, and evolution of the earth–moon system. *Advances in Geophysics,* Vol. 38, Academic Press, 179–266.
Kunze, E., and T. B. Sanford, 1996: Abyssal mixing: Where it is not. *J. Phys. Oceanogr.,* **20,** 2286–2296.
Ledwell, J. R., A. J. Watson, and C. S. Law, 1993: Evidence for slow mixing across the pycnocline from an open-ocean tracer-release experiment. *Nature,* **364,** 231–246.
Levitus, S., 1994: *World Ocean Atlas 1994*: CD-ROM Data Set Documentation. NODC Informal Rep. No. 13, 30 pp.
Loder, J. W., and C. Garrett, 1978: The 18.6-year cycle of sea surface temperature in shallow seas due to variations in tidal mixing. *J. Geophys. Res.,* **83** (C4), 1967–1970.
Lueck, R., and R. Reid, 1984: On the production and dissipation of mechanical energy in the ocean. *J. Geophys. Res.,* **89,** 3439–3445.
Lupton, J. E., J. R. Delaney, H. P. Johnson, and M. K. Tivey, 1985: Entrainment of deep-ocean water by buoyant hydrothermal plumes. *Nature,* **316,** 621–623.
McDougall, T. J., and W. K. Dewar, 1999: Vertical mixing and cabbeling, in layered models. *J. Phys. Oceanogr.,* **28,** 1458–1480.
Mellor, G. L., and T. Yamada, 1982: Development of a turbulent closure model for geostrophica fluid problems. *Rev. Geophys. Space Phys.,* **20** (4), 851–875.
Miller, G. R., 1966: The flux of tidal energy out of the deep oceans. *J. Geophys. Res.,* **71,** 2485–2489.
Monin, A. S., and A. M. Yaglom, 1971: *Statistical Fluid Mechanics: Mechanics of Turbulence.* Vol. 1. The MIT Press, 769 pp.
Morrison, L. V., 1978: Tidal decelerations of the earth's rotation deduced from astronomical observations in the period AD 1600 to the present. *Tidal Friction and the Earth's Rotation,* P. Brosche and J. Sundermann, Eds., Springer-Verlag, 22–27.
Morozov, E. G., 1995: Semidiurnal internal wave global field. *Deep-Sea Res.,* **42,** 135–148.
Munk, W. H., 1966: Abyssal recipes. *Deep-Sea Res.,* **13,** 707–730.
——, and C. Wunsch, 1998: The moon and mixing: Abyssal recipes II. *Deep-Sea Res.,* in press.
Oberhuber, J. M., 1993: Simulation of the Atlantic circulation with a coupled sea ice–mixed layer–isopycnal general circulation model. Part I: Model description. *J. Phys. Oceanogr.,* **23,** 808–829.
Olbers, D., and M. Wenzel, 1989: Determining diffusivities from hydrographic data by inverse methods with applications to the Circumpolar Current. *Oceanic Circulation Models: Combining Data and Dynamics,* L. T. Anderson and J. Willebrand, Eds., Kluwer Academic, 95–139.
Osborn, T. R., 1980: Estimates of the local rate of diffusion from dissipation measurements. *J. Phys. Oceanogr.,* **10,** 83–89.
Pacanofski, R. C., and G. Philander, 1981: Parameterization of vertical mixing in numerical models of the tropical ocean. *J. Phys. Oceanogr.,* **11,** 1442–1451.
Polzin, K. L., J. M. Toole, J. R. Ledwell, and R. W. Schmitt, 1997: Spatial variability of turbulent mixing in the abyssal ocean. *Science,* **276,** 93–96.
Rossby, H. T., 1965: On thermal convection driven by non-uniform heating from below; An experimental study. *Deep-Sea Res.,* **12,** 9–16.
Royer, T., 1993: High-latitude oceanic variability associated with the 18.6-year nodal tide. *J. Geophys. Res.,* **98,** 4639–4644.
Sandstrom, J. W., 1916: Meteorologische Studien im schwedischen Hochgebirge. *Goteborgs K. Vetensk. Vitterhets-Samh Handl., Ser. 4,* **22** (2), 48 pp.
Sjoberg, B., and A. Stigebrandt, 1992: Computations of the geographical distribution of the energy flux to mixing processes via internal tides and the associated vertical circulation in the ocean. *Deep-Sea Res.,* **39,** 269–291.
Stein, C. A., and S. Stein, 1992: A model for the global variation in oceanic depth and heat flow with lithospheric age. *Nature,* **359,** 123–129.
——, ——, and A. M. Pelayo, 1995: Heat flow and hydrothermal circulation. *Seafloor Hydrothermal Systems: Physical, Chemical, Biological, and Geological Interactions, Geophys. Monogr.,* No. 91, Amer. Geophys. Union, 425–445.
Toole, J. M., K. L. Polzin, and R. W. Schmitt, 1994: Estimates of diapycnal mixing in the abyssal ocean. *Science,* **264,** 1120–1123.
Winton, M., 1996: The role of horizontal boundaries in parameter sensitivity and decadal-scale variability of coarse-resolution ocean general circulation models. *J. Phys. Oceanogr.,* **26,** 289–304.
Weaver, A. J., and T. M. C. Houghes, 1992: Stability and variability of the thermohaline circulation and its link to climate. *Trends Phys. Oceanogr.,* **1,** 15–70.
——, E. S. Sarachik, and J. Marotzke, 1991: Freshwater flux forcing of decadal and inter-decadal oceanic variability. *Nature,* **353,** 836–838.
——, J. Marotzke, P. F. Cummins, and E. S. Sarachik, 1993: Stability and variability of the thermohaline circulation. *J. Phys. Oceanogr.,* **23,** 39–60.
Wunsch, C., 1998: The work done by the wind on the oceanic general circulation. *J. Phys. Oceanogr.,* **28,** 2331–2339.
Yin, F. L., and E. S. Sarachik, 1994: An efficient convective adjustment scheme for ocean general circulation models. *J. Phys. Oceanogr.,* **24,** 1425–1430.